ESCUELA DE CONSTRUCCIÓN CIVIL
FACULTAD DE INGENIERÍA
Revista de la Construcción
Journal of Construction

Research Article

Effective net area of failure in steel plates subjected to tension

Néstor I. Prado[1], *, Julián Carrillo[2], Claudia Retamoso[3]

[1] Faculty of Civil Engineering, Universidad Pontificia Bolivariana, Bucaramanga (Colombia); nestor.prado@upb.edu.co
[2] Department of Civil Engineering, Universidad Militar Nueva Granada, Bogotá (Colombia); julian.carrillo@unimilitar.edu.co
[3] Faculty of Civil Engineering, Universidad Pontificia Bolivariana, Bucaramanga (Colombia); claudia.retamoso@upb.edu.co
*Correspondence: nestor.prado@upb.edu.co (N. Prado)

Received: 01.06.23; **Accepted:** 28.08.24; **Published:** 12.12.24

Citation: Prado, N., Carrillo, J., and Retamoso, C. (2024). Effective net area of failure in steel plates subjected to tension. Revista de la Construcción. Journal of Construction, 23(3), 608-622. https://doi.org/10.7764/RDLC.23.3.608

Graphical Abstract:

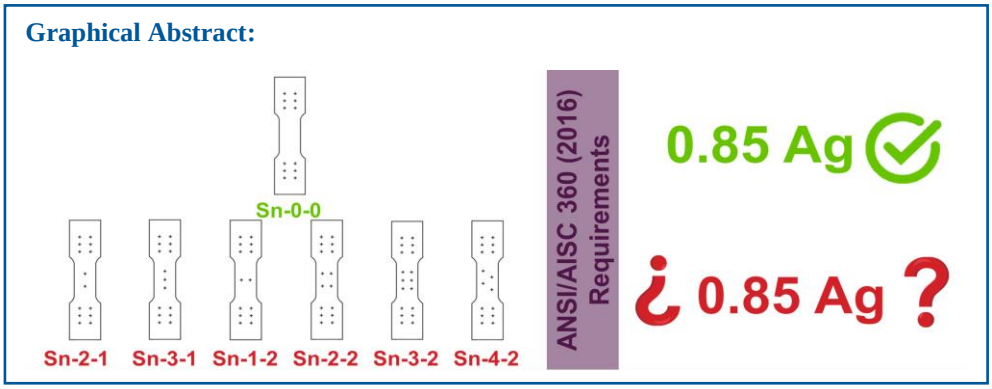

Highlights:

- 85% gross area requirements on ANSI/AISC 360 are suitable for specimens undrilled.
- 85% gross area criteria on ANSI/AISC 360 may be unconservative for drilled specimens.
- The effective net area of failure was compared with the effective net area of design.
- The failure gross area percentage is related to the slenderness ratio of the specimen.

Abstract: The current design of plates in tension due to the limit state in tensile rupture according to the requirements outlined in ANSI/AISC 360 (2016) establishes that the effective net area value (Ae), must be the net area value (An), but did not be greater than 0.85 of the gross area (Ag) of the element. The research aim was to evaluate the experimental behavior of the effective net area of failure concerning 0.85Ag of steel plates subjected to tension load conduct to reliable or unsafe design. Thirty-five specimens of A36 steel with different arrangement of holes were tensile tested. Five different plates thicknesses were considered from 3.1 mm (1/8") up to 9.5 mm (3/8"). The behavior of the effective net area of failure is discussed in term of the slenderness ratio of steel plate, the effective net area of design and analyzed based on current design specifications.

The results showed that the effective net area of failure of the undrilled specimens presented a slight tendency to increase with increasing slenderness ratio. In the specimens with two rows of holes and staggered holes this tendency decreased. Whereas for the specimens with one rows of holes the effective net area of failure did not present a clear behavior with respect to slenderness ratio. Moreover, the undrilled specimens of this study developed an effective net area of failure greater than the effective net area of design, satisfying the design specifications. But in the specimens with holes the effective net area of design was greater, generating unreliable designs. In other words, the 0.85Ag value was found adequate for the specimens without holes. Nevertheless, this value was high for the specimens with holes in this experimental research.

Keywords: tension plates, steel plates, effective net area, bolted connections, staggered bolts.

List of abbreviations:

Ae - effective net area

An - net area

Ag - gross area

Fy - yield strength

Fu - ultimate strength

Pn - theoretical load

ϕ - resistance factors for tension and tensile rupture

B - width of test specimen

t - thickness of test specimen

R - correlation coefficient

1. Introduction

In past decades, experimental and numerical research on steel plates subjected to tension load have been carried out to evaluate their behavior. Chesson and Munse (1963) performed test of riveted and bolted steel connections of plates and rolled shapes to comparison of predicted and actual efficiencies. This research concluded that the load capacity is a function of the geometry of the member, the arrangement of bolt holes and the method of fabrication. The load capacity is expressed in terms of the net section area. Fisher et al. (1978) presented statistical information relative to the development of treatment of connections based on the Load and Resistance Factor Design approach. The study showed that current design values provide significantly different levels of reliability. A set of finite element studies on the influence of staggered holes patterns in tension members was conducted by Epstein and Gulia (1993). Results indicated that the requirement design do not adequately represent the phenomenon of staggered holes to evaluate of design load.

Barth et al. (2002) studied the effect of connection eccentricity and connection length on the load capacity to tension of tees shape members (WT members-cut from W shapes). The numerical simulation results of this study exhibited an excellent concordance with the experimental failure capacities of the specimens with large connection eccentricities. In their experimental research, Može et al. (2007) focused the net cross-section failures of plates with holes and bolted connections to determine their local ductility and resistance. The influence of staggered bolt patterns was not considered in this research.

Može and Beg (2010) evaluated experimentally tension splices of steel plates with bolts in double shear to determine ductility and resistance of this connections. This research concluded that a low ultimate strength to yield strength ratio does not affect local ductility substantially. But does not allow the yielding of the gross area, and therefore the effective net area check is importance. Wei et al. (2015) studied on the fracture behavior of bolted steel tensile connections with various bolt arrangements. The study showed that the prediction of load may be can conservative for specimens with staggered holes. A new fast approach to predict the net-tension failure strength of multi-bolt composite joints was proposed by Peng et al. (2021). This approach was developed based on finite fracture mechanics and parametric finite element methods. Lin et al. (2021a) and Lin et al. (2021b) assessed experimental and numerical on net section resistance of high strength steel staggered bolted connections subjected to tension. Jiang et al. (2020) studied experimental and numerical of the structural behavior and resistance of high strength steel double shear bolted connections subjected to tension.

Di et al. (2024) and Mahmood et al. (2020) suggested that in some cases the ANSI/AISC 360 (2016) specifications overestimate the design forces, remaining above the results obtained experimentally, which is reviewed the coefficients in the current regulations for the design of elements of structural steel is relevant. Wang and Zhu (2023) highlight the importance of making experimental comparisons with American and European specifications, for a safe analysis coefficients used in the design of steel structures. The previous research has studied the subject of tension bolted connections with the objective of evaluating and predicting efficiency, the effect of connection eccentricity, the influence of staggered holes, the ductility and resistance, to predict the net-tension failure, among others. However, the literature review showed that the behavior of effective net area of failure of steel plates subjected to tension load have not been evaluated with respect to their slenderness ratio.

Therefore, this work focuses on the experimental evaluation of steel plates subjected to tension load to analyze the behavior of effective net area of failure with respect to slenderness ratio of steel plate, defined as the ratio between the width of the steel plate and its thickness as highlighted in Lin et al. (2024) and Liu et al. (2023). Also, to analyze the values of the effective net area of failure based on current design specification.

2. Experimental program

The experimental program of this research was carried out at the Universidad Pontificia Bolivariana in Bucaramanga, Colombia. Thirty-five (35) A36 steel plates specimens were tensile tested. The plate thicknesses considered were 3.1 mm (1/8”), 4.8 mm (3/16”), 6.4 mm (1/4”), 7.9 mm (5/16”) and 9.5 mm (3/8”). Fig. 1 shows the bolt hole arrangement of tests specimens for each plate thickness. One and two rows of holes were analyzed, and for each row one to three hole were considered. A specimen with staggered bolts hole was also included. All bolt holes were 14.3 mm (9/16”) in diameter, corresponding to the use of bolts 12.7 mm (1/2”) in diameter. The bolt holes were drilled.

The distribution of the holes is proposed in this way as in the literature review because they are the most common bolted connections for plates (Lin et al., 2021a; Lin et al., 2021b; Nethercot et al. 2021; Teh and Uz, 2016; Wang et al. 2019). The designation of the tests specimens of this study was based on letters and numbers, which represent thickness of specimen, number of bolt hole per row and number of rows. For example, S6.4-3-2 means 6.4 mm (1/4”) thick tests specimen, 3 bolt holes per row and 2 rows of bolt hole.

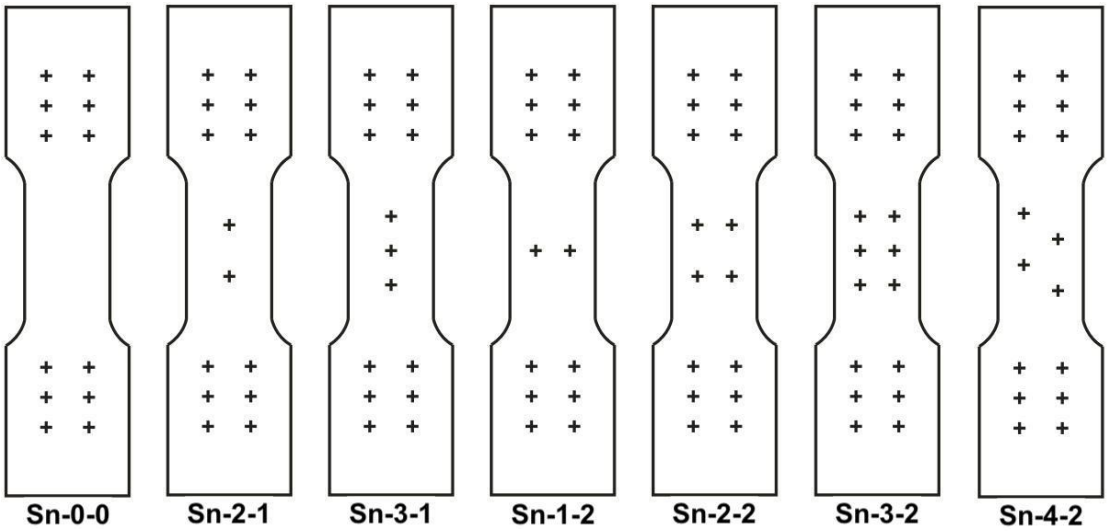

Figure 1. Arrangement of test specimens.

Fig. 2 shows the geometric details of tests specimens. The length and width of the test zone were 160 mm and 100 mm, respectively to allow the enough space of pitch and gauge of bolt holes. Whereas the dimensions of the connection zone were 175 mm and 144 mm to avoid failure of the specimens in this area. A radius of curvature of 47 mm was considered to make a transition between the test zone and the connection zone like in the research of Kamarudin et al. (2020) and Lin et al. (2024).

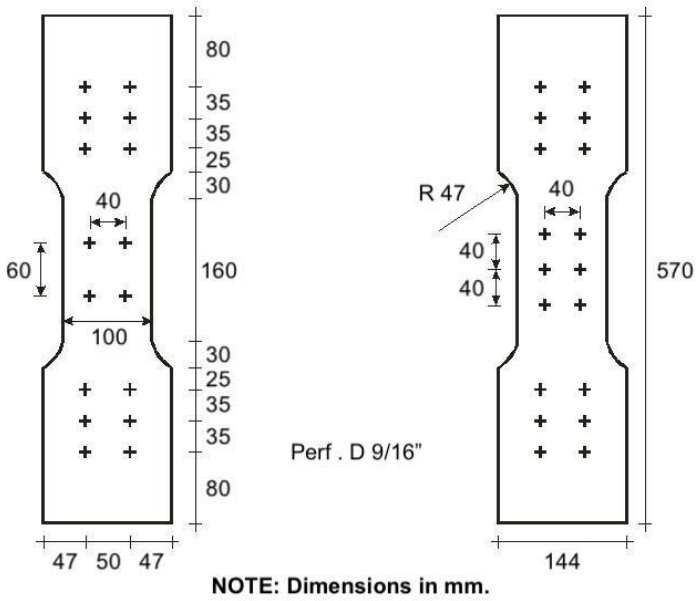

Figure 2. Geometric details of test specimens.

3. Test setup and instrumentation

The typical test setup is shown in Fig. 3. The specimens were tested in a 500 kN capacity universal testing machine.

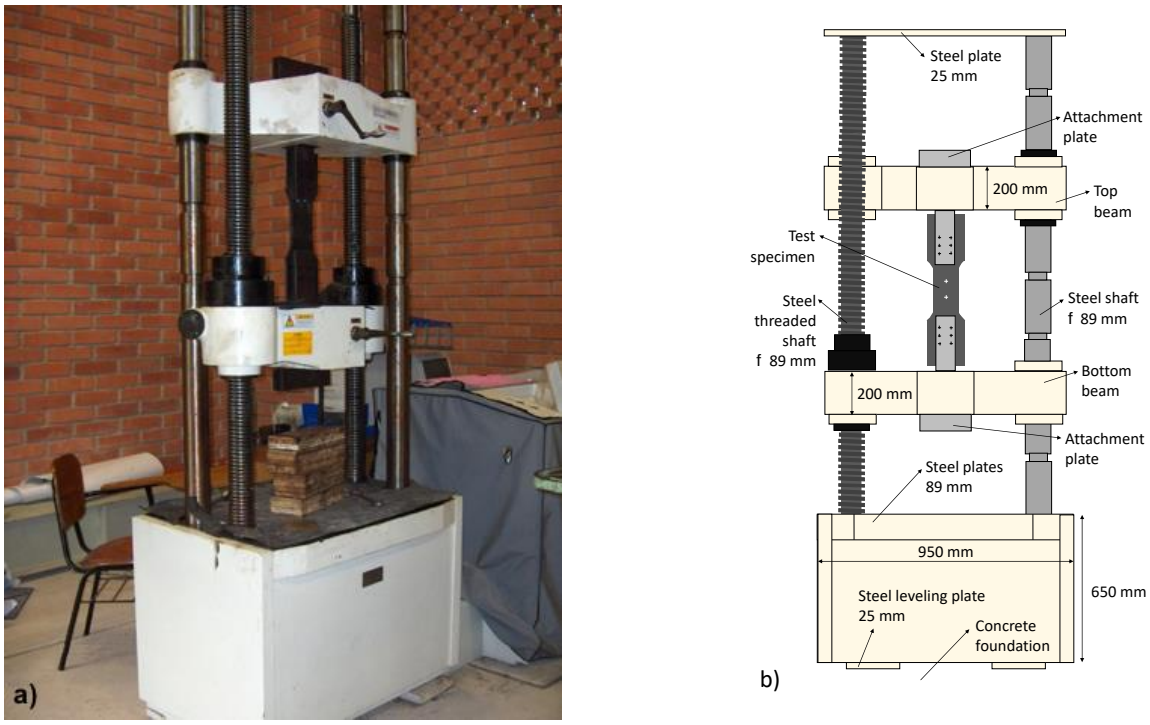

Figure 3. Universal testing machine. a) General view; b) Scheme.

All specimens were tested applying a tensile load at the ends of the plate samples. A couples of attachment plates of A50 steel were necessary to fix the tests specimens to universal machine, whose geometry and dimensions are shown in Fig. 4.

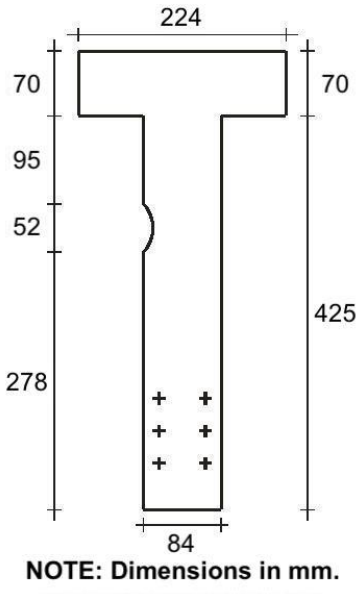

Figure 4. Geometric and dimensions of attachment plates.

The attachment plates are 19.1 mm (3/4”) thick and were designed for the limit states of tensile yielding, tensile rupture, block shear rupture, shear rupture of bolt, bearing at bolt holes, shear yielding and shear rupture. The coupling with the universal machine was achieved adding the pair of the attachment plates at the top beam and other pair at bottom beam of the universal machine as shown in Fig. 5.

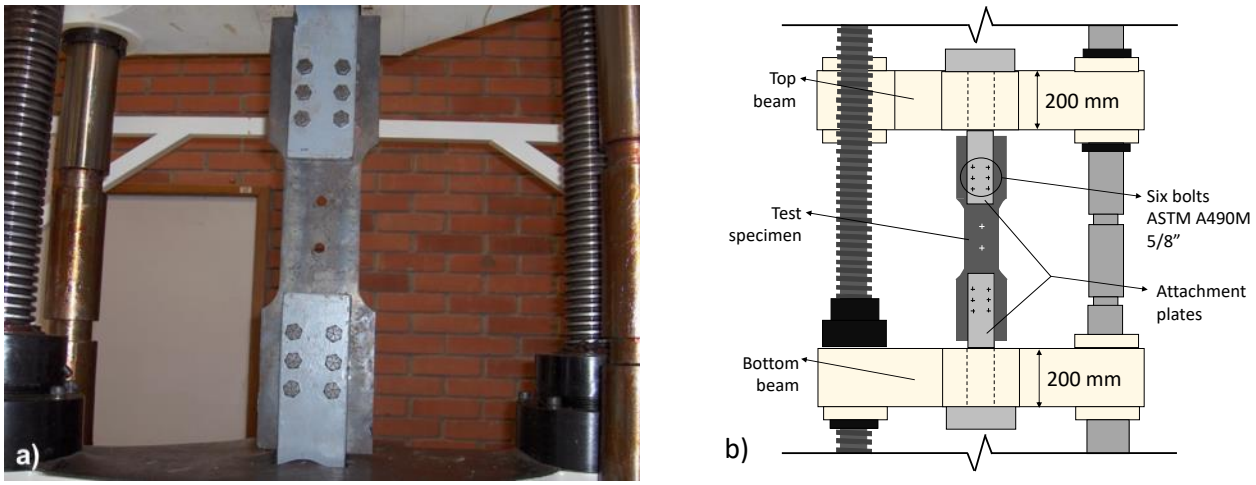

Figure 5. Detail of attachment plates to test specimen. a) General view; b) Scheme coupling of attachment plates to universal machine.

For the upper attachment plates, it was necessary to make a lateral cut in the form of an arc due to the presence of the endless screw of the universal machine. Six bolts ASTM A490M 15.9 mm (5/8”) in diameter were used to connect the attachment plates to each end of tests specimens. A built-in load cell of the universal testing machine was used to record the load applied tensile to all test specimens. The tensile load during the tests were applied with a rate of 4 mm/min until load of failure was reached (Shi et al., 2023). The rate is in order of allow an adequate redistribution of the stresses in the inelastic interval of the material (Santos et al., 2020).

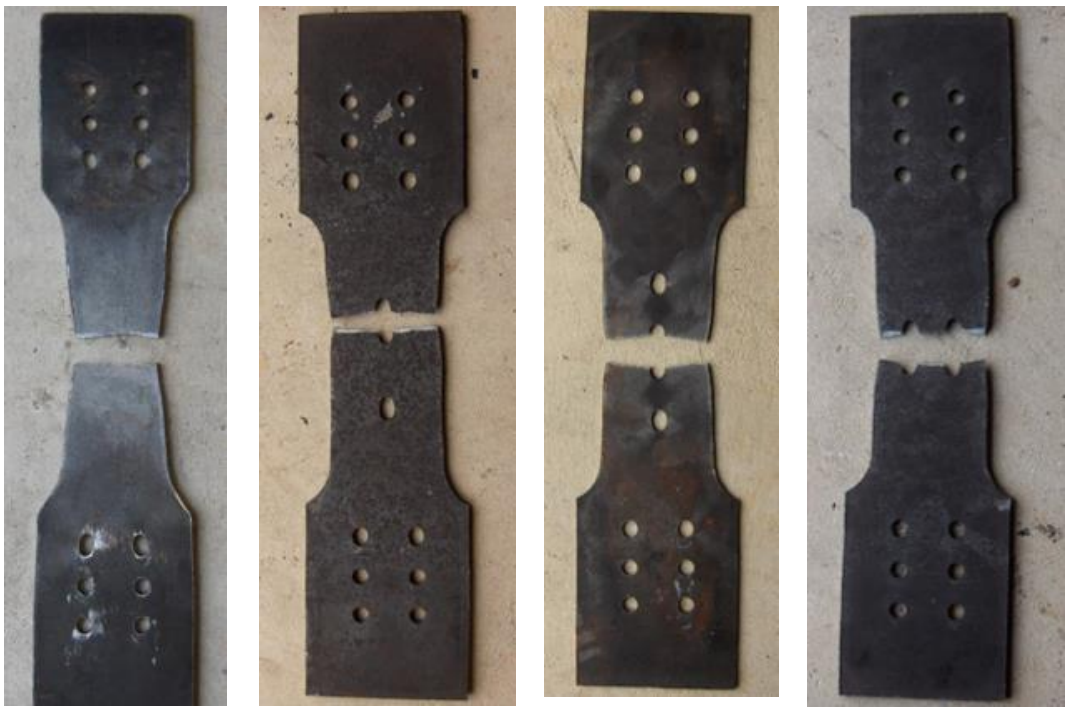

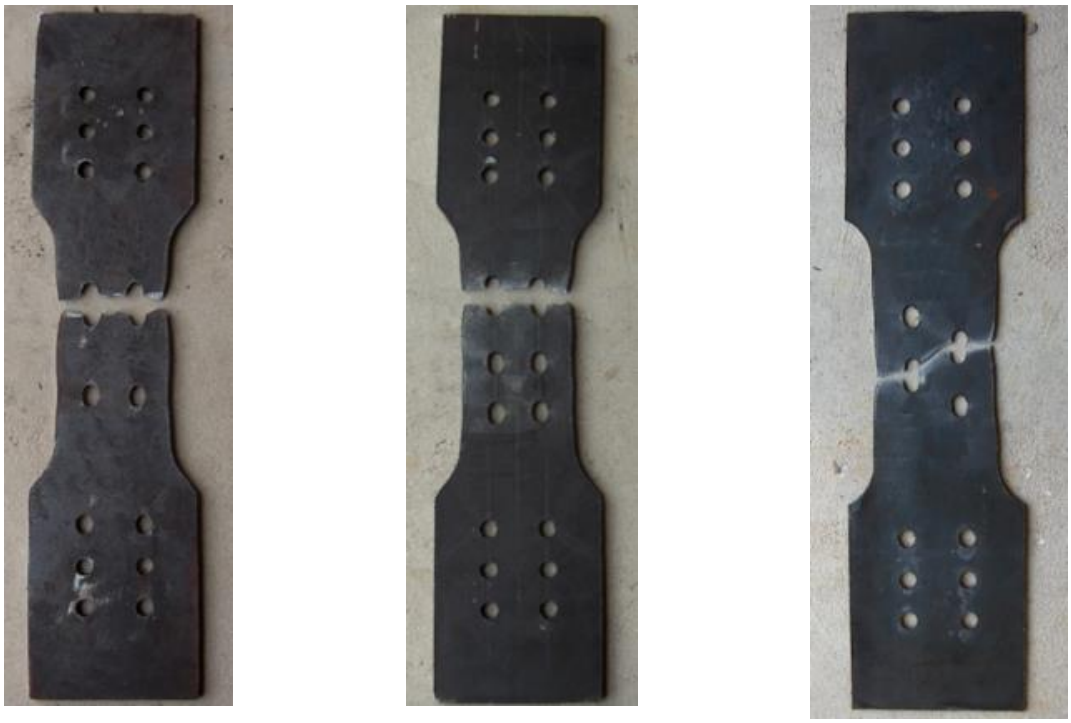

Figure 6. Failure path of the test specimens.

Fig. 6 shows the failure path of the test specimens of 6.4 mm (1/4") thick. Similar failure paths were observed for the other thicknesses of tests specimens. All failure shown concordance with respect to capacity calculated along net section fracture, especially the tests specimens with staggered net section fracture. According to Lin et al. (2021a), the same type of failure was observed in the plates as shown in Fig. 6. Table 1 shows the values of the theoretical and measured load of failure. The theoretical values were calculated according to equations 1 and 2 and the requirements outlined in chapter D of ANSI/AISC 360 (2016). In addition, Table 1 shows the values of the gross area, the net area, 85% of net area and the effective net area theoretical of each of the test specimens.

Based on the limit state tensile rupture (equation 2), the effective net area of failure was obtained by dividing the measured load of failure by the ultimate strength of the A36 steel (fu = 400 MPa). It is worth noting that the effective net area theoretical is the value of the lowest area that controls the limit state tensile rupture according to the specifications outlined in ANSI/AISC 360 (2016).

$$\phi P_n = \phi f_y A_g \quad (1)$$

$$\phi P_n = \phi f_u A_e \quad (2)$$

Where the resistance factors for tension and tensile rupture were taken as 1.0, for comparison purposes with the experimental failure load; the effective net area value (Ae) must be the net area value (An), but it must not be greater than 0.85 of the gross area (Ag) of the member. The net area value was equal to the gross area minus the hole area on the failure path.

Table 1. Values of theoretical and measured failure load.

Test Specimens	Ag (cm^2)	An (cm^2)	An/Ag	0.85 Ag (cm^2)	Ae-theorical (cm^2)	Ae-failure (cm^2)	Ae-failure/Ag	Theoretical load (kN)	Failure load (kN)
S3.1-0-0	3.10	3.10	1.00	2.64	2.64	3.00	0.97	105.6	119.8
S3.1-2-1	3.10	2.66	0.86	2.64	2.64	2.39	0.77	105.6	95.5
S3.1-3-1	3.10	2.66	0.86	2.64	2.64	2.44	0.79	105.6	97.5
S3.1-1-2	3.10	2.21	0.71	2.64	2.21	2.17	0.70	88.4	86.8
S3.1-2-2	3.10	2.21	0.71	2.64	2.21	1.89	0.61	88.4	75.4
S3.1-3-2	3.10	2.21	0.71	2.64	2.21	2.06	0.67	88.4	82.5
S3.1-4-2	3.10	2.39	0.77	2.64	2.39	1.94	0.63	95.6	77.5
S4.8-0-0	4.80	4.80	1.00	4.08	4.08	4.08	0.85	163.2	163.1
S4.8-2-1	4.80	4.11	0.86	4.08	4.08	3.81	0.79	163.2	152.5
S4.8-3-1	4.80	4.11	0.86	4.08	4.08	4.00	0.83	163.2	160.1
S4.8-1-2	4.80	3.43	0.71	4.08	3.43	3.19	0.66	137.2	127.6
S4.8-2-2	4.80	3.43	0.71	4.08	3.43	3.06	0.64	137.2	122.5
S4.8-3-2	4.80	3.43	0.71	4.08	3.43	2.77	0.58	137.2	110.8
S4.8-4-2	4.80	3.70	0.77	4.08	3.70	3.18	0.66	148.0	127.1
S6.4-0-0	6.40	6.40	1.00	5.44	5.44	5.71	0.89	217.6	228.4
S6.4-2-1	6.40	5.49	0.86	5.44	5.44	5.16	0.81	217.6	206.4
S6.4-3-1	6.40	5.49	0.86	5.44	5.44	5.06	0.79	217.6	202.3
S6.4-1-2	6.40	4.57	0.71	5.44	4.57	4.53	0.71	182.8	181.2
S6.4-2-2	6.40	4.57	0.71	5.44	4.57	4.47	0.70	182.8	178.7
S6.4-3-2	6.40	4.57	0.71	5.44	4.57	4.72	0.74	182.8	188.6
S6.4-4-2	6.40	4.93	0.77	5.44	4.93	4.53	0.71	197.2	181.0
S7.9-0-0	7.90	7.90	1.00	6.72	6.72	8.71	1.10	268.8	348.4
S7.9-2-1	7.90	6.77	0.86	6.72	6.72	7.40	0.94	268.8	296.0
S7.9-3-1	7.90	6.77	0.86	6.72	6.72	7.08	0.90	268.8	283.2
S7.9-1-2	7.90	5.64	0.71	6.72	5.64	6.63	0.84	225.6	265.0
S7.9-2-2	7.90	5.64	0.71	6.72	5.64	6.38	0.81	225.6	255.2
S7.9-3-2	7.90	5.64	0.71	6.72	5.64	6.35	0.80	225.6	254.1
S7.9-4-2	7.90	6.09	0.77	6.72	6.09	6.42	0.81	243.6	256.8
S9.5-0-0	9.50	9.50	1.00	8.08	8.08	8.32	0.88	323.2	332.9
S9.5-2-1	9.50	8.14	0.86	8.08	8.08	7.22	0.76	323.2	288.9
S9.5-3-1	9.50	8.14	0.86	8.08	8.08	6.95	0.73	323.2	278.1
S9.5-1-2	9.50	6.79	0.71	8.08	6.79	8.02	0.84	271.6	320.8
S9.5-2-2	9.50	6.79	0.71	8.08	6.79	8.04	0.85	271.6	321.5
S9.5-3-2	9.50	6.79	0.71	8.08	6.79	8.08	0.85	271.6	323.3
S9.5-4-2	9.50	7.32	0.77	8.08	7.32	7.99	0.84	292.8	319.5

4. Experimental results and discussion

4.1. Behavior of the effective net area of each specimen thickness

Fig. 7 shows for all tests specimens, the values of theoretical net area (gray column) and the effective net area of failure (black column). At the top of the columns, the values of theoretical net area and the effective net area of failure were expressed as percentage of the gross area. The above to compare them with the value of 85% of gross area.

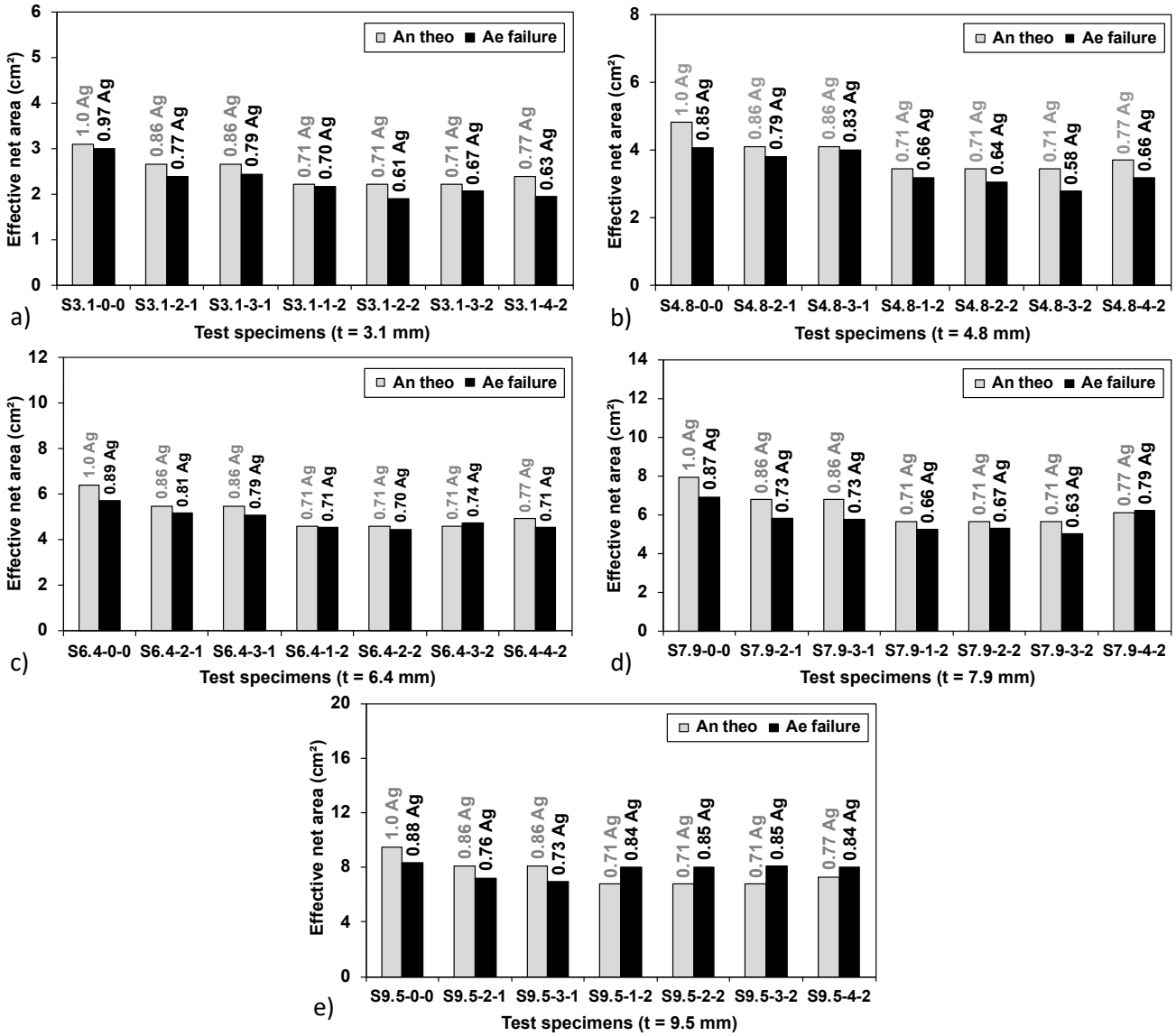

Figure 7. Effective net area of specimens. a) Specimens with t = 3.1 mm; b) Specimens with t = 4.8 mm; c) Specimens with t = 6.4 mm; d) Specimens with t = 7.9 mm; e) Specimens with t = 9.5 mm.

The effective net area of failure of all specimens without holes ranged from 85% to 97% of gross area. These values were greater and equal than 85% of gross area, which according to requirements outlined in ANSI/AISC 360 (2016), is taken as the value of effective net area of design. These results confirm that the requirement to limit the value of the effective net area of design to 85% of the gross area is adequate for undrilled specimens, since the failure load should not be lower than the design load. Whereas in the research of Teh et al. (2011), the area reduction factor proposed by the AISC is in the appropriate range and meets the experimental specifications of plates with bolted connections, as was observed in the results of this project.

Moreover, the specimens with one row of holes presented a theoretical net area of 86% of gross area. Therefore, the effective net area of design was controlled by 85% of the gross area according to requirements outlined in ANSI/AISC 360 (2016). But the values of the effective net area of failure of these test specimens ranged from 73% to 83% of gross area. That is, no one of the 10 test specimens complied with the requirement, given that the failure load of all test specimens was lower than the design load. Zureick and Nassar (2024) found experimentally that the coefficients for calculating the net load on the

effective cross-section are below the findings in the tests. This suggests that these coefficients should be updated to ensure the safety of bolted connections in metal structures.

On the other hand, the theoretical net area of all test specimens with two rows of holes was 71% of gross area and for the test specimens with staggered holes was 77% of gross area. These values were lower than 85% of gross area. Hence, the effective net area of design was taken equal to the theoretical net area. Nevertheless, the effective net area of failure of the test specimens with two rows of holes ranged from 58% to 85% of gross area. Whereas for the test specimens with staggered holes ranged from 63% to 84% of gross area. Sayed (2021) was found that the ANSI/AISC 360 (2016) reduction coefficients for the net section are greater than those found experimentally, and a reduction of this value is suggested in the regulations, like in this investigation.

By comparing the effective net area of failure with respect to the effective net area of design, only 7 of the 30 drilled test specimens complied the requirements outlined in ANSI/AISC 360 (2016). The test specimens that complied the requirements were S6.4-1-2, S6.4-3-2, S7.9-4-2, S9.5-1-2, S9.5-2-2, S9.5-3-2 and S9.5-4-2. These results suggest that the requirement to limit the effective net area of design to 85% of gross area might be unconservative for drilled specimens. It would be convenient to study the possibility of reducing this value to ensure that the design load to be less than the failure load (Sayed, 2021).

4.2. Behavior of the percentage of gross area with respect to slenderness ratio of the test specimens

Fig. 8 shows the values of percentage of gross area of failure according to the slenderness ratio and hole arrangement of the test specimens. The slenderness ratio is defined as the ratio between the width of the test zone of the specimen and its thickness.

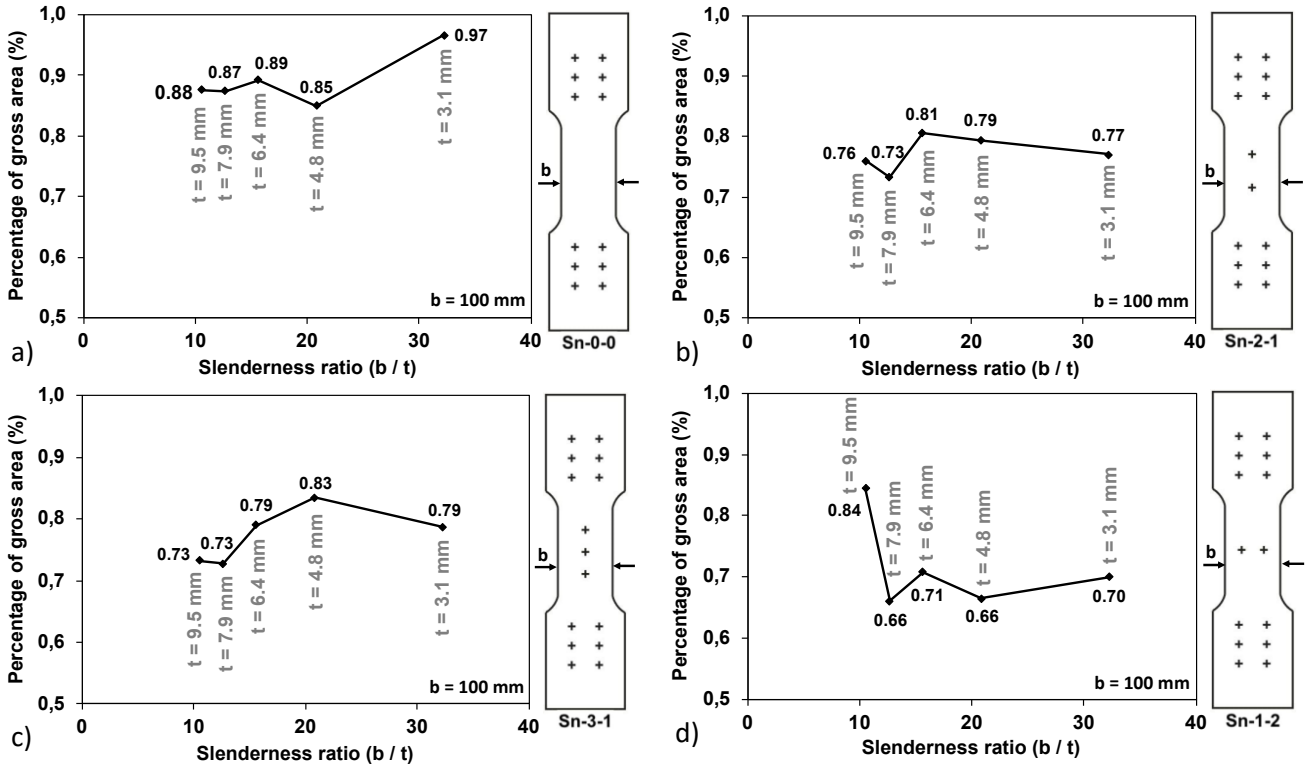

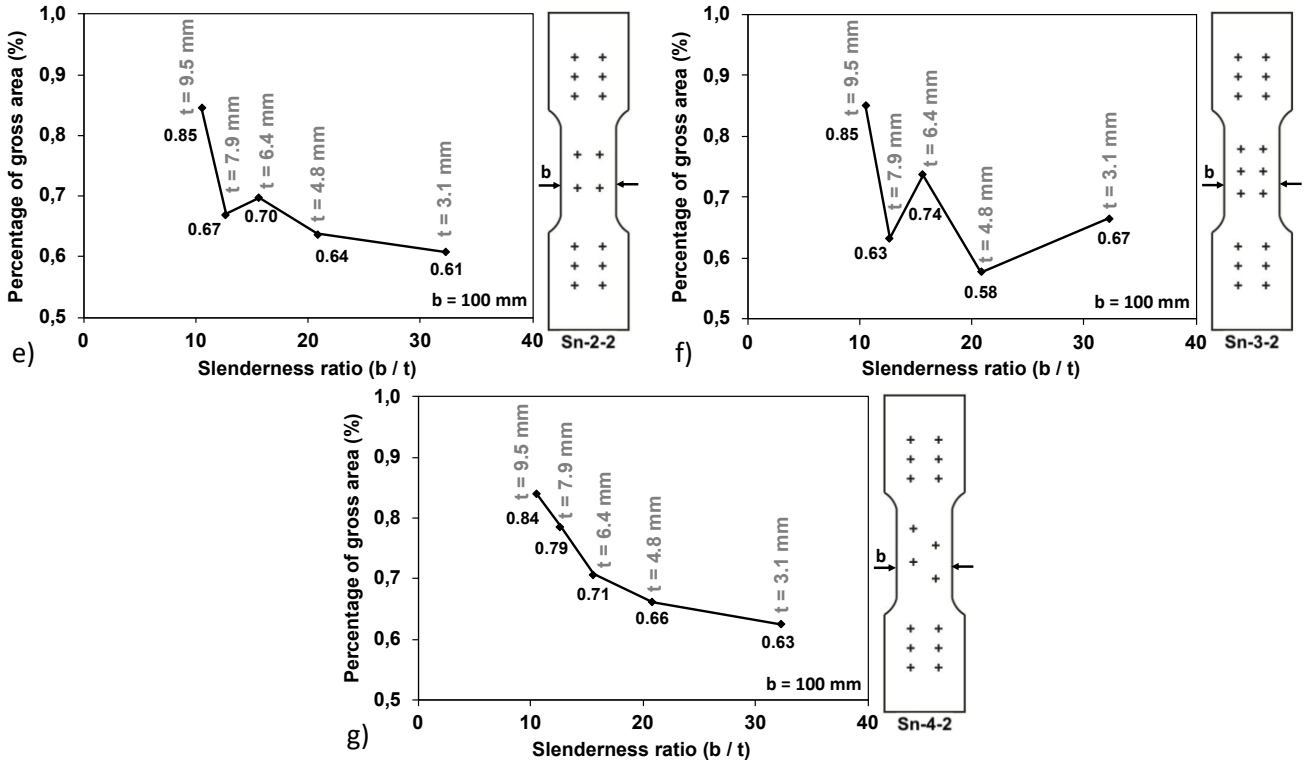

Figure 8. Percentage of gross area vs slenderness ratio. a) Specimens Sn-0-0; b) Specimens Sn-2-1; c) Specimens Sn-3-1; d) Specimens Sn-1-2; e) Specimens Sn-2-2; f) Specimens Sn-3-2; g) Specimens Sn-4-2.

The percentage of gross area of failure of the test specimens without holes presented a slight tendency to increase with increasing slenderness ratio (Fig. 8a). In other words, the percentage of gross area of failure increase when the thickness of test specimens decreases. This could be associated with a better distribution of tensile stress in the cross area of the test specimens avoiding stress peaks. For the test specimens with one row of holes, the percentage of gross area of failure did not present a clear tendency to increase or decrease with increasing slenderness ratio as shown in Fig. 8b and 8c. It could be considered that the percentage of gross area of failure maintained a relatively constant behavior. Whereas for the specimens with two rows of holes the percentage of gross area of failure exhibited a tendency to decrease with increasing slenderness ratio as shown in Fig. 8d-8f. The percentage of gross area of failure of the test specimens with staggered holes presented a clear tendency to decrease when increase the slenderness ratio as shown in Fig. 8g.

4.3. Behavior of the effective net area of failure with respect to number of holes per row

Fig. 9 shows the values of effective net area of failure agree to number of holes per row and the thickness of test specimens. The results indicated that there is no correlation or tendency in the variables.

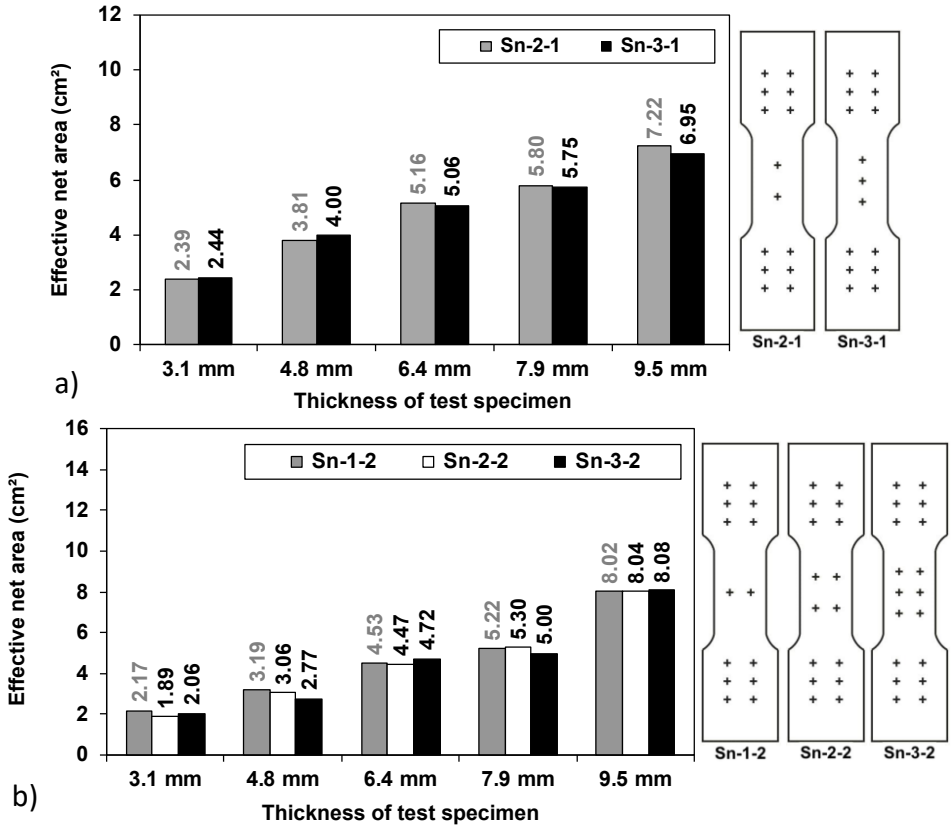

Figure 9. Effective net area of failure vs. thickness of test specimens. a) Specimens with one row of holes; b) Specimens with two rows of holes.

4.4. Response surface analysis of holes per row and plate thickness

The response surface analysis method lets it know the relationship between two factors with an effect in specified limits (Hu et al., 2023; NIST/SEMATECH, 2012). Moreover, in the specific case, the number of perforations and the thickness of the plates (mm) will be related. Therefore, a coefficient concerning the response was obtained, as the relationship between the effective net area of failure (Ae-failure) and gross area (Ag).

Applying the methodology to solve the coefficients, the equation (3) was obtained where x_1 is the thickness of the plates in mm, x_2 is the number of holes in each row, and y is the Ae-failure/Ag ratio (NIST/SEMATECH, 2012).

$$y = \beta_0 + \beta_1 \cdot x_1 + \beta_2 \cdot x_2 + \beta_3 \cdot x_1^2 + \beta_4 \cdot x_2^2 + \beta_5 \cdot x_1 \cdot x_2 \quad (3)$$

$$y = 0.8215 + 0.01496 \cdot x_1 - 0.1344 \cdot x_2 - 0.00022 \cdot x_1^2 + 0.01748 \cdot x_2^2 + 0.00429 \cdot x_1 \cdot x_2$$

The limits of the x_1 and x_2 are 0 to 4 holes and 3.1 to 9.5 mm thickness, respectively. It is important to clarify that the four holes refer to the sample with staggered perforations. The relationship between the experimental data and the response surface is measured with the correlation coefficient R^2 = 53.11%. The residuals between the response surface and the experimental data had a normal fit with a linear regression adjusted with an R^2 of 96.42% (NIST/SEMATECH, 2012).

According to the results of this research, it was observed in Fig. 10, that for the specimens with one (1) bolt hole per row, the coefficient of effectiveness of the gross area is between 0.75 and 0.80 in thicknesses between 3.1 and 5.3 mm, between 0.80 and 0.85 for thicknesses between 5.3 and 8.4 mm, and between 0.85 and 0.90 for thicknesses between 8.4 and 9.1 mm.

For two (2) bolt holes, the coefficient was found to be between 0.65 and 0.70 with thicknesses between 3.1 and 3.4 mm, between 0.70 and 0.75 for thicknesses between 3.4 and 5.7 mm, between 0.75 and 0.80 for thicknesses between 5.7 and 8.1 mm, and between 0.80 and 0.85 for thicknesses between 8.1 and 9.1 mm. For three (3) bolt holes, the coefficient is between 0.65 and 0.70 for thicknesses between 3.1 and 4.6 mm, between 0.70 and 0.75 for thicknesses between 4.6 and 6.6 mm, between 0.75 and 0.80 for thicknesses between 6.6 and 8.6 mm, and between 0.80 and 0.85 for thicknesses between 8.6 and 9.1 mm.

For the specimens with staggered holes the coefficient of effectiveness of the net area is between 0.65 and 0.70 for thicknesses between 3.1 and 4.2 mm, between 0.70 and 0.75 for thicknesses between 4.2 and 6.1 mm, between 0.75 and 0.80 for thicknesses between 6.1 and 7.8 mm, and between 0.80 and 0.85 for thicknesses between 7.8 and 9.1 mm. Finally, from the results of the response surface analysis it was observed that for the specimens with 2, 3, and staggered holes, all coefficients are less than 0.85 Ag established by the requirements described in the ANSI/AISC 360 (2016). It is suggested that further studies be carried out in this regard, to better correlate the coefficient with the number of holes and the thickness, thus achieving a more conservative design.

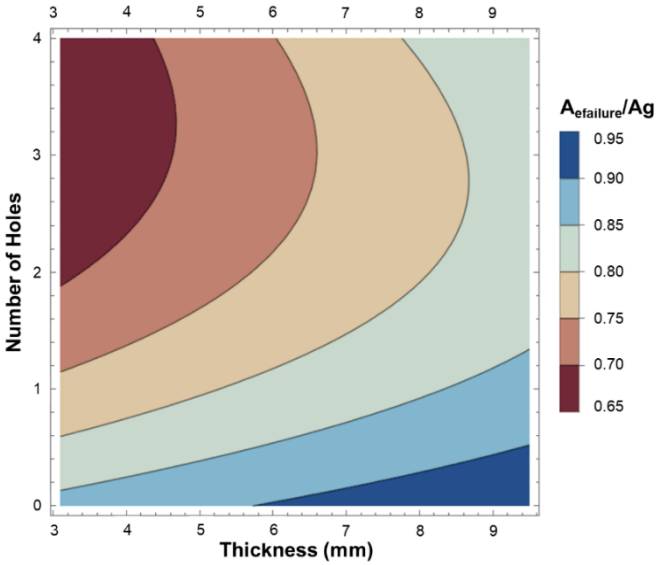

Figure 10. Ae-failure/Ag ratio-dependent on the thickness of the plate and the number of holes per row.

5. Conclusions and comments

A set of conclusions are drawn from the results of this testing program:

1. The performed tests in this research showed that the specimens undrilled developed an effective net area of failure greater to effective net area of design. Therefore, the requirements outlined in ANSI/AISC 360 (2016) are suitable to specimens without holes. These specimens reached values of effective net area of failure between 85% to 97% of gross area, greater to 85% of gross area, expected smallest value.
2. Nevertheless, 23 of the 30 drilled specimens developed an effective net area of failure lower than effective net area of design, which is taken as the lowest between the theoretical net area and the 85% of gross area. Hence, the requirements outlined in ANSI/AISC 360 (2016) are not fully met. These results suggest that the requirement to limit the effective net area of design to 85% of gross area might be unconservative for drilled specimens. It would be convenient to carry out more test to study the possibility of reducing this value to ensure that the design load to be less than the failure load.

3. In addition, the percentage of gross area of failure of the test specimens without holes presented a slight tendency to increase with increasing slenderness ratio when the thickness of test specimens decreases. Whereas for the specimens with two rows of holes the percentage of gross area of failure exhibited a tendency to decrease.
4. On the other hand, all test specimens with staggered holes presented a clear decrease in the percentage of gross area of failure when increase the slenderness ratio. For the test specimens with one row of hole, a clear behavior of these variables was not evidenced.

Author contributions: The contribution of the authors is equitable.

Funding: The authors would like to thank the Universidad Pontificia Bolivariana Bucaramanga for the financial support for supplying the steel plates for this project referenced with the number 038-0705-2300.

Conflicts of interest: The authors confirm that there is not conflict of interest.

References

ANSI/AISC_360-16. (2016). Specification for Structural Steel Buildings. In American Institute of Steel Construction.

Barth, K. E., Orbison, J. G., and Nukala, R. (2002). Behavior of steel tension members subjected to uniaxial loading. Journal of Constructional Steel Research, 58, 1103–1120. www.elsevier.com/locate/jcsr

Chesson, E. J., and Munse, W. H. (1963). Riveted and Bolted Joints: Truss-Type Tensile Connections. Journal of the Structural Division, 89(1).

Di, J., Xiao, B., Li, Y., Su, Y., and Zhang, Q. (2024). Failure Modes and Bearing Capacity of High-Strength–Steel-Bearing-Type Bolted Connections. Journal of Structural Engineering, 150(3). https://doi.org/10.1061/jsendh.steng-12814

Epstein, H. I., and Gulia, F. S. (1993). Finite Element Studies of Bolt Stagger Effects in Tension Members. Computers and Structures, 48(6), 1153–1156.

Fisher, J. W., Galambos, T. V., Kulak, G. L., and Ravindra, M. K. (1978). Load and Resistance Factor Design Criteria for Connectors. Journal of the Structural Division, 104(9).

Hu, H., Song, W., Song, G., and Li, Y. (2023). Optimization design and parametric research of belt conveyor deck truss structure. Structures, 57. https://doi.org/10.1016/j.istruc.2023.105155

Jiang, K., Zhao, O., and Tan, K. H. (2020). Experimental and numerical study of S700 high strength steel double shear bolted connections in tension. Engineering Structures, 225. https://doi.org/10.1016/j.engstruct.2020.111175

Kamarudin, A. F., Musa, M. K., Mokhatar, S. N., Tuan Chik, T. N., Mohd Zuki, S. S., Abu Bakar, A., Hadipramana, J., and Ahmad Johari, H. H. (2020). Mechanical Properties of Single Shear Plane of Bolted Steel Connection. IOP Conference Series: Materials Science and Engineering, 713(1). https://doi.org/10.1088/1757-899X/713/1/012031

Lin, X. M., Yam, M. C. H., Chung, K. F., Ke, K., and He, Q. (2021). Experimental and numerical study on net section resistance of high strength steel staggered bolted connections. Engineering Structures, 247. https://doi.org/10.1016/j.engstruct.2021.113111

Lin, X. M., Yam, M. C. H., Chung, K. F., and Lam, A. C. C. (2021). A study of net-section resistance of high strength steel bolted connections. Thin-Walled Structures, 159. https://doi.org/10.1016/j.tws.2020.107284

Lin, X. M., Yam, M. C. H., Song, Y., Chung, K. F., Ho, H. C., and Han, Y. (2024). Net section tension capacity of high strength steel single shear bolted connections. Thin-Walled Structures, 195. https://doi.org/10.1016/j.tws.2023.111371

Liu, S., Feng, R., and Zhong, C. (2023). Shear Performance of Steel Thin Sheet-to-Thick Plate Bolted Connections. International Journal of Steel Structures, 23(4), 962–973. https://doi.org/10.1007/s13296-023-00745-z

Mahmood, M., Elamin, A., and Tizani, W. (2020). Ultimate strength and fracture sequence of bolted connections to thin-walled carbon steel. Structures, 23, 646–659. https://doi.org/10.1016/j.istruc.2019.11.011

Može, P., and Beg, D. (2010). High strength steel tension splices with one or two bolts. Journal of Constructional Steel Research, 66(8–9), 1000–1010. https://doi.org/10.1016/j.jcsr.2010.03.009

Može, P., Beg, D., and Lopatič, J. (2007). Net cross-section design resistance and local ductility of elements made of high strength steel. Journal of Constructional Steel Research, 63(11), 1431–1441. https://doi.org/10.1016/j.jcsr.2007.01.009

Nethercot, D. A., Salih, E. L., and Gardner, L. (2011). Behaviour and Design of Stainless Steel Bolted Connections. Advances in Structural Engineering, 14(4), 647–658.

NIST/SEMATECH. (2012). Engineering Handbook of Statistical Methods. National Institute of Standards and Tech-nology - U.S. Department of Commerce, 1(1).

Peng, X., Li, X., Liu, G., and Zhao, J. (2021). Prediction of net-tension failure of multi-bolt composite joints: A fast approach for laminates with arbitrary layup. European Journal of Mechanics, A/Solids, 87. https://doi.org/10.1016/j.euromechsol.2021.104213

Santos, A. F., Santiago, A., Latour, M., Rizzano, G., and Simões da Silva, L. (2020). Response of friction joints under different velocity rates. Journal of Constructional Steel Research, 168. https://doi.org/10.1016/j.jcsr.2020.106004

Sayed, A. M. (2021). Tensile Capacity of Steel Plate Connections with Different Bolt Distribution due to Tensile Load. Journal of Engineering Science and Technology, 16(2), 888–902.

Shi, D., Huang, H., Li, N., Liu, Y., and Demartino, C. (2023). Bolted steel to laminated timber and glubam connec-tions: Axial behavior and finite-element modeling. International Journal of Mechanical Sciences, 252. https://doi.org/10.1016/j.ijmecsci.2023.108364

Teh, L. H., Asce, A. M., and Gilbert, B. P. (2011). Net Section Tension Capacity of Bolted Connections in Cold-Reduced Steel Sheets. Journal of Structural Engineering, 138(3), 337–344. https://doi.org/10.1061/(ASCE)ST.1943-541X

Teh, L. H., and Uz, M. E. (2016). Combined Bearing and Shear-Out Capacity of Structural Steel Bolted Connections. Journal of Structural Engineering, 142(11). https://doi.org/10.1061/(asce)st.1943-541x.0001573

Wang, L., and Zhu, X. (2023). Bearing Behavior of Cold-Formed Thick-Walled Steel Plates with a Single Bolt. Applied Sciences (Switzerland), 13(12). https://doi.org/10.3390/app13126897

Wang, Y. B., Lyu, Y. F., Li, G. Q., and Liew, J. Y. R. (2019). Bearing-strength of high strength steel plates in two-bolt connections. Journal of Constructional Steel Research, 155, 205–218. https://doi.org/10.1016/j.jcsr.2018.12.011

Wei, F., Fang, C., Yam, M. C. H., and Zhang, Y. (2015). Fracture behaviour and design of steel tensile connections with staggered bolt arrangements. International Journal of Steel Structures, 15(4), 863–879. https://doi.org/10.1007/s13296-015-1208-4

Zureick, A.-H., and Nassar, C. (2024). Influence of Bolt Threads on the Net Section Tensile Rupture Strength of Sin-gle-Bolt Connections in Pultruded Structures. Journal of Composites for Construction, 28(4). https://doi.org/10.1061/jccof2.cceng-4537